PIECEMEAL CALDERA COLLAPSE AS THE TRIGGER OF CHAOTIC TERRAINS AND FLOOR-FRACTURED CRATERS ON THE MOON AND MARS. E. Luzzi[1], A.P. Rossi[1], M. Massironi[2], R. Pozzobon[2], D. Maestrelli[3], G. Corti[3]
[1]Department of Physics and Earth Sciences, Jacobs University Bremen, Germany (e.luzzi@jacobs-university.de) [2]Dipartimento di Geoscienze, Università degli Studi di Padova, Italy, [3]CNR-IGG, The National Research Council of Italy, Institute of Geosciences and Earth Resources, Florence, Italy

Introduction: The formation mechanism of the enigmatic chaotic terrains on Mars has been at the center of a long-lasting debate in the last decades. The most accepted hypotheses include groundwater overpressure within a confined aquifer [1][2][3][4], melting of a buried icy lake [5][6][7], interactions between magma and ice or water [8][9][10], and instability of a large amount of underground clathrates [11]. In these proposed scenarios, water (either liquid or ice) is often playing a major role in the trigger of the collapse. [12] observed that fluvial evidences were missing in Arsinoes and Pyrrhae Chaos, as well as an outflow channel, pre- and syn-collapse hydrated minerals and any clue suggesting that before and during the collapse the area was water-rich. Instead, a variety of tectono-volcanic features were found by the authors. In addition, similar features occur within Floor-Fractured craters (FFCs) on Mars and on the Moon, where groundwater is not present; magmatic processes are instead the common ground between Mars and the Moon.

On Earth, a type of caldera collapse called *piecemeal* or *chaotic* is known to produce the collapse of an area where radial and concentric faults intersect each other generating polygonal blocks [13]. The goal of our experiments was to test (a) if it was possible to obtain the geometries observed in chaotic terrains and FFCs through a pure magmatic process, without interaction with water; (b) if length, depth and angles of the faults in the models were consistent.

Data and methods: The experiments consisted in multiple cycles of inflation and deflation of an analogue magma chamber, underlying fine granular sands, where at each cycle the polyglicerine acting as magma was intruded and then withdrawn. Two setups were build: one with a circular magma chamber, to be compared to FFCs (called S1, Fig. 1-A), and one with an irregular elliptical shape, to be compared to Arsinoes Chaos (called S2, fig. 1-C,D,E,F).

At the end of each intrusion/withdrawal stereo images were taken to produce Digital Elevation Models (DEMs), through the software Metashape.

These measurements were then compared to Arsinoes Chaos and an unnamed FFC on Mars using a CTX mosaic [14] and HRSC-MOLA blended DEMs [15], and to the lunar FFC Komarov crater using a LROC WAC image [16] and a LOLA-SELENE blended DEM [17]. The models were correctly scaled (both geometric and dynamic scaling), so that 1 cm in the model corresponds to 20 km in Arsinoes Chaos and 10 km in FFCs.

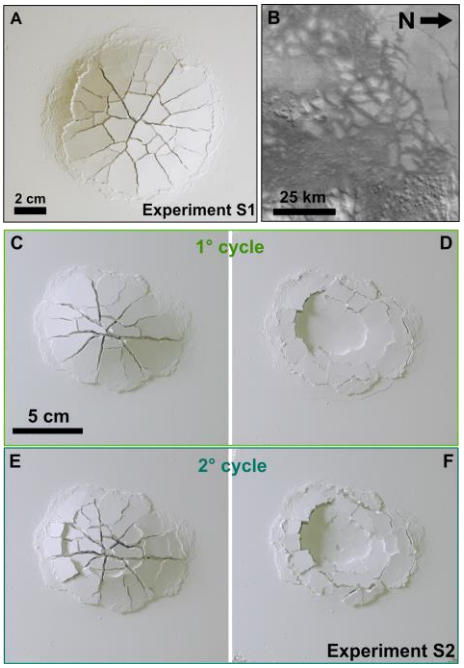

Fig. 1: (A) Experiment S1; (B) Arsinoes Chaos, Mars (CTX mosaic); (C) Experiment S2, first inflation; (D) Experiment S2. First deflation; (E) Experiment S2, second inflation; (F) Experiment S2, second deflation.

Experimental results and implications: In both the experiments, with the first inflation the bulging begins accompanied by the formation of radial dilational faults and concentric thrusts bordering the periphery of the buried magma chamber (Fig. 1-B). During the first deflation (Fig. 1-C), at the end of the withdrawing, the bulge collapses, the thrusts are reactivated as normal faults and the outermost concentric normal faults are identified as the ring fault system, while other concentric faults combined with the previously formed radial faults produce the polygonal geometries bounding the angular blocks. At the second inflation (Fig. 1-D) more radial dilational faults are produced and the bulge grows but presents a collapsed top. The cycles end with the second deflation (Fig. 1-E), a major subsidence affects the ring fault, new radial and

Scaled Parameters (1:10)	Experiment **S1** (after second cycle)	**Unnamed FFC** (Mars)	**Komarov crater** (Moon)
Magma chamber perimeter	28.6 cm (286 km)	?	?
Magma chamber depth	0.5 cm (5 km)	?	?
Radial faults (max length)	4.6 cm (46 km)	40 km	51 km
Radial faults (average length)	3 cm (30 km)	20 km	30 km
Ring fault perimeter	30 cm (300 km)	240 km	280 km
Ring fault subsidence	0.45 cm (4.5 km)	1-2 km	1-3 km
Concentric periphery faults (max length)	8.2 cm (82 km)	34 km	53 km
Concentric periphery faults (average length)	7.6 cm (76 km)	32 km	45.5 km
Average angle between fractures	95°	95°	95°

Scaled Parameters (1:20)	Experiment **S2** (after second cycle)	**Arsinoes Chaos** (Mars)
Magma chamber perimeter	46 cm (920 km)	?
Magma chamber depth	0.6 cm (12 km)	?
Radial faults (max length)	4.6 cm (92 km)	40 km
Radial faults (average length)	3.6 cm (72 km)	27 km
Ring fault perimeter	27 cm (540 km)	593 km
Ring fault subsidence	0.15 cm (3 km)	1-4 km
Concentric periphery faults (max length)	6.3 cm (160 km)	87 km
Concentric periphery faults (average length)	4.7 cm (94 km)	60.5 km
Average angle between fractures	97°	95°

Table 1: comparison of the measurements between models and natural cases

concentric structures form, and the pre-existing are enhanced.

The structures formed during the piecemeal collapse fit with the geometries identified on chaotic terrains and FFCs. The qualitative comparisons are shown in Figure 2, while quantitatively results are reported in Table 1.

Despite the complexity in the natural case on Mars is increased by millions years of erosion and by the occurrence of sedimentary infillings in the central part of the chaos, the similarity between our models and the natural cases leads to question the effectiveness of the water as primary agent for the collapse.

Acknowledgments: We acknowledge support and funding from the European Union's Horizon 2020 research and innovation programme under grant agreement N°776276 (PLANMAP).

References: [1] Andrews-Hanna J.C., and Phillips, R. J. (2007). *JGR: Planets, 112*(E8). [2] Harrison, K. P., & Grimm, R. E. (2009). *JGR: Planets, 114*(E4). [3] Rodriguez, J. A. P. et al. (2005). *Icarus, 175*(1), 36–57. [4] Warner, N. H. et al. (2011). *JGR, 116*(E6). [5] Manker, J. P., & Johnson, A. P. (1982). *Icarus, 51*(1), 121–132. [6] Roda, M., et al. (2014). *Icarus, 236*, 104–121. [7] Zegers, T. E. et al. (2010). *EPSL, 297*(3–4), 496–504. [8] Head, J. W., & Wilson, L. (2017). *Icarus, 283*, 176–223. [9] Leask, H. J. et al. (2006). *JGR: Planets, 111*(E8). [10] Meresse, S. et al. (2008). *Icarus, 194*(2), 487–500. [11] Kargel, J. S. et al. (2007). *Geology, 35*(11), 975–978. [12] Luzzi, E. et al. (2020). *JGR: Planets, 125*. [13] Troll, V. R., et al. (2002). *Geology, 30*(2), 135–138. [14] Dickson, J. et al. (2018). *LPSC, 49*, 1-2. [15] Fergason, R. L. et al. (2018). *US Geological Survey*. [16] Robinson, M. S. et al. (2010). *SSR, 150*(1–4), 81–124. [17] LOLA team and Kaguya Team (2015). *PDS, Goddard Space Flight Center*.

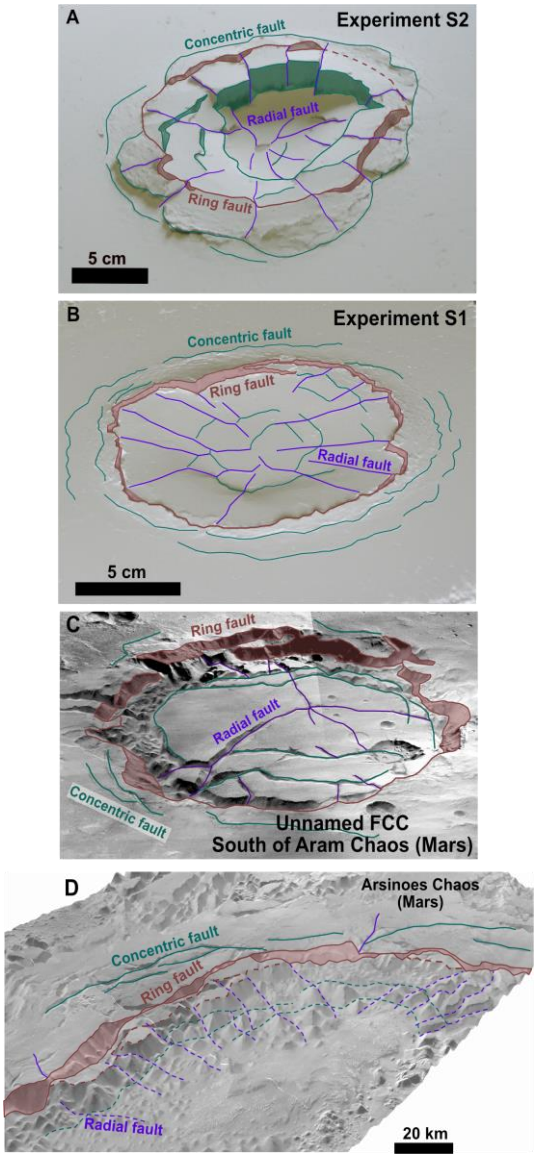

Fig. 2: (A) Experiment S2 and line-drawing of the structures; (B) Experiment S2 and line-drawing of the structures; (C) Unnamed FFC on Mars and line-drawing of the structures (CTX mosaic) ; (D) Arsinoes Chaos, Mars (CTX mosaic)